Journal of Inorganic Biochemistry 199 (2019) 110796

Contents lists available at ScienceDirect

Journal of Inorganic Biochemistry

journal homepage: www.elsevier.com/locate/jinorgbio

Cation and peptide binding properties of CML7, a calmodulin-like protein from *Arabidopsis thaliana*

Matteo Trande[a], Marco Pedretti[a], Maria Cristina Bonza[b], Adele Di Matteo[c], Mariapina D'Onofrio[a], Paola Dominici[a], Alessandra Astegno[a,*]

[a] Department of Biotechnology, University of Verona, Strada Le Grazie 15, 37134 Verona, Italy
[b] Department of Biosciences, University of Milano, Via Celoria 26, 20133 Milano, Italy
[c] Institute of Molecular Biology and Pathology, CNR, Piazzale Aldo Moro 5, Roma 00185, Italy

ARTICLE INFO

Keywords:
Calmodulin-like proteins
Calcium sensor
EF-hand
Arabidopsis thaliana
Melittin

ABSTRACT

Plants contain a large family of so-called calmodulin-like proteins (CMLs) which differ from canonical calmodulin in that they show greater variability in sequence, length, and number of EF-hand domains. The presence of this extended CML family has raised questions regarding the role of these proteins: are they functionally redundant or do they play specific functions in physiological plant processes? To answer these questions, comprehensive biochemical and structural information on CML proteins is fundamental. Among the 50 CMLs from *Arabidopsis thaliana*, herein we described the ability of CML7 to bind metal ions focusing on the Ca^{2+} and Mg^{2+} sensing properties, as well as on metal-induced conformational changes. Circular dichroism and nuclear magnetic resonance (NMR) studies indicated that both Ca^{2+} and Mg^{2+} stabilize CML7, as reflected in conformational rearrangements in secondary and tertiary structure and in increases in thermal stability of the protein. However, the conformational changes that binding induces differ between the two metal ions, and only Ca^{2+} binding controls a structural transition that leads to hydrophobic exposure, as suggested by 8-anilino-1-naphthalenesulfonic acid fluorescence. Isothermal titration calorimetry data coupled with NMR experiments revealed the presence of two high affinity Ca^{2+}-binding sites in the C-lobe of CML7 and two weaker sites in the N-lobe. The paired nature of these CML7 EF-hands enables them to bind Ca^{2+} with positive cooperativity within each globular domain. Our results clearly place CML7 in the category of Ca^{2+} sensors. Along with this, the protein can bind to a model target peptide (melittin) in a Ca^{2+}-dependent manner.

1. Introduction

In plants, calcium (Ca^{2+}) ions play key roles in the regulation of many physiological processes. A significant diversity and abundance of proteins that bind Ca^{2+} using the EF-hand, an evolutionarily preserved helix-loop-helix motif, have evolved in plants, including calmodulin (CaM) and calmodulin-like proteins (CMLs). CaMs and CMLs are largely considered to act as Ca^{2+} sensors that can mediate cellular responses through a well-known mechanism in which the Ca^{2+}-bound form of these proteins can interact with specific downstream targets to modulate cellular activity [1].

After plant genome sequencing projects were completed, the presence of a multitude of genes predicted to encode either identical or highly homologous isoforms of CaM and various CMLs has emerged as a typical feature in plants. CaM/CML gene families are represented by seven CaM and 50 CML genes in *Arabidopsis thaliana* [2] and five CaM and 32 CML genes in rice [3]. Additionally, lists of CaM and CML genes have been identified in many vegetable and fruit crops, such as tomato, [4], strawberry [5], grapevine [6], and cabbage [7]. Interestingly, while CaMs are well-conserved in all eukaryotes, the CML family is unique to the plant kingdom. Similarly to CaM, CMLs are characterized by the presence of EF-hand motifs and no other known functional domains [2].

The presence of a large CML family in plants has raised fundamental and still open questions regarding the evolutionary selection in preserving such apparently redundant family in the plant genome. To this end, the CML field has experienced an explosion of investigations in the last years, mainly focused on: i) elucidation of the metal binding ability and the structural features of CMLs [8–14]; ii) identification of specific targets of CMLs as well as the processes in which they are involved [10,15–22]; iii) determination of the expression patterns and regulation at the protein and messenger RNA levels during different processes, e.g.

* Corresponding author.
E-mail address: alessandra.astegno@univr.it (A. Astegno).

https://doi.org/10.1016/j.jinorgbio.2019.110796
Received 9 April 2019; Received in revised form 26 July 2019; Accepted 31 July 2019
Available online 01 August 2019

plant development or response to external stimuli [4–7,23]. Acquired knowledge has provided evidence that CMLs are not a simple CaM safety backup system; rather, they are likely to play specific functions in coordinating plant responses to endogenous and environmental stimuli. However, although significant insights into the function and regulation of various CMLs have been provided, and a holistic view of how the CML genes function at different levels is emerging, how this family can contribute to cellular signaling and still maintain properties that are dissimilar from CaM and other Ca^{2+} sensors is still elusive.

Accumulating evidence suggests that the biochemical properties of individual CMLs, such as the number of Ca^{2+} binding sites, cooperativity, metal affinity, capacity to distinguish between Ca^{2+} and other physiological ions (i.e. Mg^{2+}), and conformational rearrangement upon binding to metal ions are crucial parameters that contribute to the specificity of various Ca^{2+} mediated responses. Sequence divergence among CMLs may lead to different binding properties, creating diverse subsets of CMLs capable of perceiving stimulus-specific Ca^{2+} signals and regulate specific targets, thus coupling the perception of different signals to precise physiological responses. In this light, the comparison of the Ca^{2+} binding and structural properties of CMLs which are related to conserved eukaryotic CaM with those more divergent from CaM may help to distinguish between specificity and redundancy in the plant CaM/CML families.

According to a recent phylogenetic analysis performed taking into the account the occurrence of CaM and CML proteins in the genomes of the green lineage [24], CMLs recognized as being closely related to CaMs (subgroup Ia) were distributed to subgroups Ib and Ic, while CMLs that diverge more from conserved CaMs could be categorized in seven subgroups (from II to VIII). Herein, we investigated the isoform CML7 from *A. thaliana* (At1g05990). Interestingly, even if CML7 has been classified as a member of subgroup VII, it possesses significant sequence similarity with CaM2 from *A. thaliana* (~ 45% of amino acid sequence identity). CML7 is a 16.9 kDa protein composed of 150 amino acid residues and characterized by four EF-hands that are predicted to be functional Ca^{2+} binding sites by PROSITE ProRule annotation [25], based on the presence of canonical Ca^{2+}-coordinating groups [26]. These observations suggest the potential capacity of CML7 to bind Ca^{2+} *in vitro*.

Functional analyses, albeit limited, have revealed that CML7 is likely involved in root development processes, in which the protein appears to act as a negative regulator, inhibiting hair tip growth [27]. However, its properties as a Ca^{2+} sensor, its downstream targets, and the mechanism of action by which CML7 can negatively transduce Ca^{2+} signals into a physiological response have not been elucidated yet.

Accordingly, we characterized CML7 from *A. thaliana* in terms of Ca^{2+} binding affinity, structural properties, and conformational perturbation upon metal binding using spectroscopic and calorimetric techniques, and we determined its subcellular localization using confocal microscopy. We examined the behavior of CML7 also in the presence of Mg^{2+}, a physiologically relevant cation that, due to its chemical properties similar to Ca^{2+} and its high concentration in plant cells (*in vivo*, cytosolic Ca^{2+} and Mg^{2+} concentrations are about 100–200 nM and 0.5–1 mM, respectively) could represent a possible Ca^{2+} competitor towards CML7 binding [28]. Moreover, we studied the interaction of CML7 with the model CaM-binding peptide melittin.

We believe that the structural information obtained in our study, in addition to the demonstration that CML7 behaves as a Ca^{2+} sensor, will help aid in better understanding the specificity of CML7 in the evolutionary panorama of the multigene family of CMLs present in plants.

2. Experimental procedures

2.1. DNA constructs

The cDNA sequence for CML7 (At1g05990) was obtained from the Arabidopsis Information Resource (TAIR) into a pUNI51 vector. The coding sequence was polymerase chain reaction (PCR)-amplified using the following primers: forward, 5′-**CATATG**GATCCGACAGAGCTAAAAC, and reverse, 5′-**GGATCC**CTACAAAGAATTAAAACCACCG. The forward primer carried a *Nde*I restriction site (bold), while the reverse primer contained a stop codon and a *Bam*HI restriction site (bold). For protein expression, the cDNA sequence was further cloned using standard laboratory protocols into pET21a vector using *Nde*I/*Bam*HI restriction sites and the plasmid construct was verified by DNA sequencing.

For CML7 subcellular localization studies, the complete coding sequence (CDS) of the red fluorescent protein (RFP) was amplified by PCR using Phusion® High-Fidelity DNA Polymerase (New England Biolabs, USA) according to the manufacturer's protocol. The following primers, forward 5′-**GCGGCCGC**GATGGCCTCCTCCGAGGACG-3′ and reverse 5′-**GCGGCCGC**TCACCCGGGTGCTCCAGTACTGT-3′ were used to add a *Not*I site (bold) to both ends of the PCR product. Following *Not*I digestion, RFP was inserted into the polylinker of the plant expression vector pGREEN0029::ter [29] under the control of the cauliflower mosaic virus (CaMV) 35S promoter (pGREEN0029::RFP). The complete CDS of CML7 was PCR amplified using forward 5′-ACG**CTCGAG**ATGGATCCGACAGAGCTAAAACG-3′ and reverse 5′-CG**GAATTC**CAAAGAATTAAAACCAC-3′ primers to add *Xho*I and *Eco*RI restriction sites (bold) at 5′ and 3′ respectively during amplification. The reverse primer also eliminates the stop codon at the 3′ of CML7 CDS. Following a *Xho*I/*Eco*RI digestion, CML7 CDS was inserted into pGREEN0029::RFP for the in frame fusion at the C-terminus with RFP. Sequencing confirmed the accuracy of the construct.

2.2. Protein production

Recombinant CML7 was expressed in *E. coli* strain BL21(DE3)pLysS (Stratagene) and purified by heat treatment and Ca^{2+}-dependent phenyl-Sepharose chromatography. Expression was induced by adding 0.4 mM isopropyl β-D-1-thiogalactopyranoside (IPTG) to 1 L of bacterial culture [pET21a-CML7] grown in LB medium supplemented with 100 μg/mL ampicillin and 34 μg/mL chloramphenicol to exponential phase and incubating at 24 °C for 16 h.

Cells were isolated by centrifugation (5000*g* for 15 min), and the pellet was resuspended in 50 mM Tris-HCl, 150 mM KCl, 0.5 mM dithiothreitol (DTT) pH 7.5 buffer containing 0.1 mg/mL lysozyme, stirred at room temperature for 30 min, and then sonicated on ice. After removing cell debris by centrifugation, the supernatant was subject to heat treatment (6 min at 85 °C followed by 40 min on ice). The precipitate was removed by centrifugation and the heat-treated lysate containing 5 mM $CaCl_2$ was loaded onto a phenyl-Sepharose column, previously equilibrated with buffer containing 50 mM Tris-HCl, 0.5 mM $CaCl_2$, 0.5 mM DTT pH 7.5. The column was then washed with the same buffer containing 150 mM KCl. CML7 was eluted in 50 mM Tris-HCl, 150 mM KCl pH 7.5, 2 mM ethylene glycol-bis(2-aminoethyl ether)-*N*,*N*,*N*′,*N*′-tetraacetic acid (EGTA) buffer. The purity of CML7 was estimated by sodium dodecyl sulfate–polyacrylamide gel electrophoresis (SDS-PAGE) analysis and the protein concentration was determined by the Bradford assay [30]. Final yield was about 20 mg/L culture.

^{15}N and ^{13}C labeled CML7 samples for NMR experiments were obtained using M9 minimal medium supplemented with 1 g/L $^{15}NH_4Cl$ and 4 g/L ^{13}C-glucose as the sole sources of nitrogen and carbon. In M9 medium the final yield was about 10 mg/L culture.

CaM1 from *A. thaliana* was produced as described [31].

2.3. Nuclear magnetic resonance

Nuclear magnetic resonance (NMR) spectra were recorded on a Bruker Avance III spectrometer (Bruker, Karlsruhe, Germany) operating at 600.13 MHz proton Larmor frequency, and equipped with a cryogenic probe. ^{1}H-^{15}N Heteronuclear Single Quantum Coherence (HSQC) experiments were recorded at 298 K on a ^{15}N labeled sample, in 50 mM

Tris-HCl, 50 mM KCl, 0.5 mM DTT, 7% D_2O pH 7.5 at protein concentration of 270 μM in the presence of EGTA (5 mM), or $MgCl_2$ (5 mM EGTA + 10 mM $MgCl_2$) or $CaCl_2$ (5 mM). The data matrix consisted of 2048 (F2, ^1H) × 256 (F1, ^{15}N) complex data points, spectral windows of 8417.509 Hz (^1H) × 2189.445 Hz (^{15}N), 8 transients, and 1.5 s relaxation delay. Standard triple resonance experiments, HNCACB, CBCA(CO)NH, and ^1H-^{15}N Nuclear Overhauser Effect SpectroscopY (NOESY) HSQC were recorded at 298 K on ^{15}N,^{13}C-labeled samples at protein concentration of 500 μM to achieve partial sequence-specific backbone atoms assignment of CML7 bound to Ca^{2+}. The HNCACB, and CBCA(CO)NH spectra were acquired with a data matrix consisting of 2 K (F3, ^1H) × 90 (F2, ^{15}N) × 120 (F1, ^{13}C) complex points, spectral windows of 8417.51 Hz (^1H) × 2189.42 Hz (^{15}N) × 11,318.16 Hz (^{13}C), 8 transients, and 1.5 s relaxation delay. The ^1H-^{15}N NOESY HSQC spectrum was acquired with a data matrix consisting of 2 K (F3, ^1H) × 40 (F2, ^{15}N) × 128 (F1, ^1H) complex points, spectral windows of 8417.51 Hz (^1H) × 2189.42 Hz (^{15}N) × 8417.51 Hz (^1H), 16 transients, and 120 ms mixing time. Data processing was performed with Topspin3.2 (Bruker, Karlsruhe, Germany).

2.4. Isothermal titration calorimetry

Isothermal titration calorimetry (ITC) experiments were performed on a TA nanocalorimeter (TA Instruments). In each experiment, 1.5 μL injections of 3 mM $CaCl_2$ were made to a 200 μL sample cell containing 200 μM of apo- or Mg^{2+}-bound CML7 in 50 mM Tris-HCl, 150 mM KCl, 0.5 mM DTT pH 7.5 buffer. Mg^{2+}-loaded CML7 was obtained by incubation of apo-protein with 10 mM $MgCl_2$ for 15 min at 25 °C. Experiments were performed at 25 °C with injections at 300-s intervals and 250 rpm stirring speed. The buffer was decalcified using a Chelex-100 ion-exchange resin (Sigma) as described [8,32] and all solutions were degassed prior to each experiment. Control experiments (injecting ligand solutions into the buffer) were conducted to obtain a baseline for each experiment and determine the heat of dilution/mixing. These values were subtracted from the experimental runs in the presence of protein. Analysis of the data was performed using Origin-based software. The reported values represent the mean ± SEM of at least three independent titrations using at least two different CML7 preparations.

2.5. Circular dichroism spectroscopy

All circular dichroism (CD) spectra were recorded on a Jasco J-1500 spectropolarimeter equipped with a thermostatically controlled Peltier type compartment, using the protocols described in [14,15,33]. Briefly, near UV (320–250 nm) and far UV (250–200 nm) spectra of ~ 100 μM and ~12 μM CML7, respectively, were collected at 25 °C after consecutive additions of 1 mM EGTA, 2 mM $MgCl_2$ and 2 mM $CaCl_2$. Quartz cuvettes were used both for near UV (1 cm) and far UV (0.1 cm). CD spectra of protein/peptide complex were obtained using a protein:peptide ratio of 1:1 in 50 mM Tris-HCl, 150 mM KCl, 0.5 mM DTT pH 7.5 in the presence of 2 mM EGTA or 2 mM $CaCl_2$. Spectra from five scans were averaged and were corrected for background signal by subtracting out the spectrum of the buffer. Denaturation profiles were recorded in the same conditions as for far UV spectra by following CD signal at 222 nm between 4 and 96 °C (scan rate 90 °C/h).

2.6. Fluorescence spectroscopy

8-Anilinonaphtalene-1-sulfonate (ANS) fluorescence spectra were measured using a Jasco FP8200 spectrofluorometer to probe the changes in hydrophobicity of CML7 following Mg^{2+} and Ca^{2+} binding, as described in [14,33]. Protein at 1 μM was incubated with 15 μM ANS and fluorescence was measured after 1 h incubation at room temperature with EGTA (2 mM), or $MgCl_2$ (0.5 mM EGTA + 5 mM $MgCl_2$) or $CaCl_2$ (2 mM). ANS fluorescence spectra were recorded at room temperature with slit widths set to 5 nm. Excitation wavelength was 380 nm and emission spectra were collected in the range 400–650 nm.

For the CML7/melittin and AtCaM1/melittin interaction the single Trp residue of melittin was excited at 295 nm, and fluorescence emission spectra were recorded with a single scan over the range 305–450 nm. Melittin (2 μM) was titrated with increasing concentrations of AtCaM1 or CML7 in 50 mM Tris-HCl, 150 mM KCl, 0.5 mM DTT pH 7.5 in the presence of 2 mM $CaCl_2$. Titration experiments were performed by monitoring the blue-shift in wavelength (λ) of the peptide emission peak. The dissociation constant (K_d) was determined according to a tight binding hypothesis [34–36]:

$$fb = \frac{\lambda - \lambda_0}{\lambda_{max} - \lambda_0} = \frac{e_0 + x + K_d - \sqrt{[(e_0 + x + K_d)^2 - 4e_0x]}}{2e_0} \quad (1)$$

where fb is the fraction bound, x is the protein concentration, e_0 is the peptide concentration, λ is the value of wavelength of the peptide emission peak as a function of protein concentration, λ_0 is the value at zero protein concentration and λ_{max} is the value at saturating protein concentration.

2.7. Limited proteolysis

CML7 at 0.5 mg/mL concentration was digested with trypsin (1:500 w/w) in 50 mM Tris-HCl, 150 mM KCl, 0.5 mM DTT pH 7.5 in the presence of 5 mM $CaCl_2$ or 5 mM EGTA, respectively, at 25 °C. At various times (0, 1, 5, 10, 20, 40, 60, 120, and 180 min), 20 μL aliquots were taken for 15% SDS-PAGE analysis. The reaction was stopped by sample boiling and addition of reducing Laemmli buffer. Bands in denaturing gel were visualized by Coomassie Blue staining.

2.8. Ca^{2+}-dependent electrophoresis mobility shift assay

CML7 recombinant protein was analyzed by SDS-PAGE (15%) or native PAGE (12%) after incubation (30 min at room temperature) with 5 mM $CaCl_2$ or 5 mM EGTA in the presence and absence of DTT, as previously described [8,14,32].

Peptide-protein stoichiometry was analyzed by incubating AtCaM1 or CML7 (20 μM) for 20 min at room temperature with increasing concentrations of melittin in 100 mM Tris-HCl pH 7.5 in the presence of 5 mM $CaCl_2$ or 5 mM EGTA, as described [33]. Samples were analyzed under native conditions on a 12% continuous gel containing 5 mM $CaCl_2$ or 5 mM EGTA.

2.9. A. thaliana protoplast isolation and transformation

Mesophyll protoplasts were isolated and transiently transformed according to [37]. Leaves from four week old *A. thaliana* Col-0 plants were collected and cut in 0.5–1 mm strips with fresh razor blades and put into multiwell cell culture in the presence of the following enzymatic plasmolysis mix: 20 mM KCl, 0.4 M D-Mannitol, 20 mM 2-(N-Morpholino)ethanesulfonic acid,4-Morpholineethanesulfonic acid (MES), 1.25% R10 Cellulase, 0.3% R10 Macerozyme. Enzymes were pre-heated at 55 °C for 10 min and 10 mM $CaCl_2$ and 0.1% bovine serum albumin (BSA) were added to the mix after the incubation. The enzymatic mix was filtered and added to the cut leaves. A 10 min vacuum favored enzymes entering the leaves through the cuticle. Digestion was performed in the dark for about 3 h without shaking. Protoplasts were separated from the cell debris by filtering the mixture through a nylon sieve of 50 μm pore size. Protoplasts were spun at 100*g* for 6 min in presence of 50 mM $CaCl_2$, washed once in cold W5 washing solution (154 mM NaCl, 125 mM $CaCl_2$, 5 mM KCl, 2 mM MES) and resuspended in the same solution. After incubation on ice for 30 min, protoplasts were resuspended in 600 μL MMg (0.4 M D-Mannitol, 15 mM $MgCl_2$, 4 mM MES pH 5.7) and centrifuged at 100*g* for 1 min. For the co-transformation with the free enhanced green fluorescent protein (EGFP), the DNA constructs (5–10 μg of pGREEN0029::CML7-RFP and

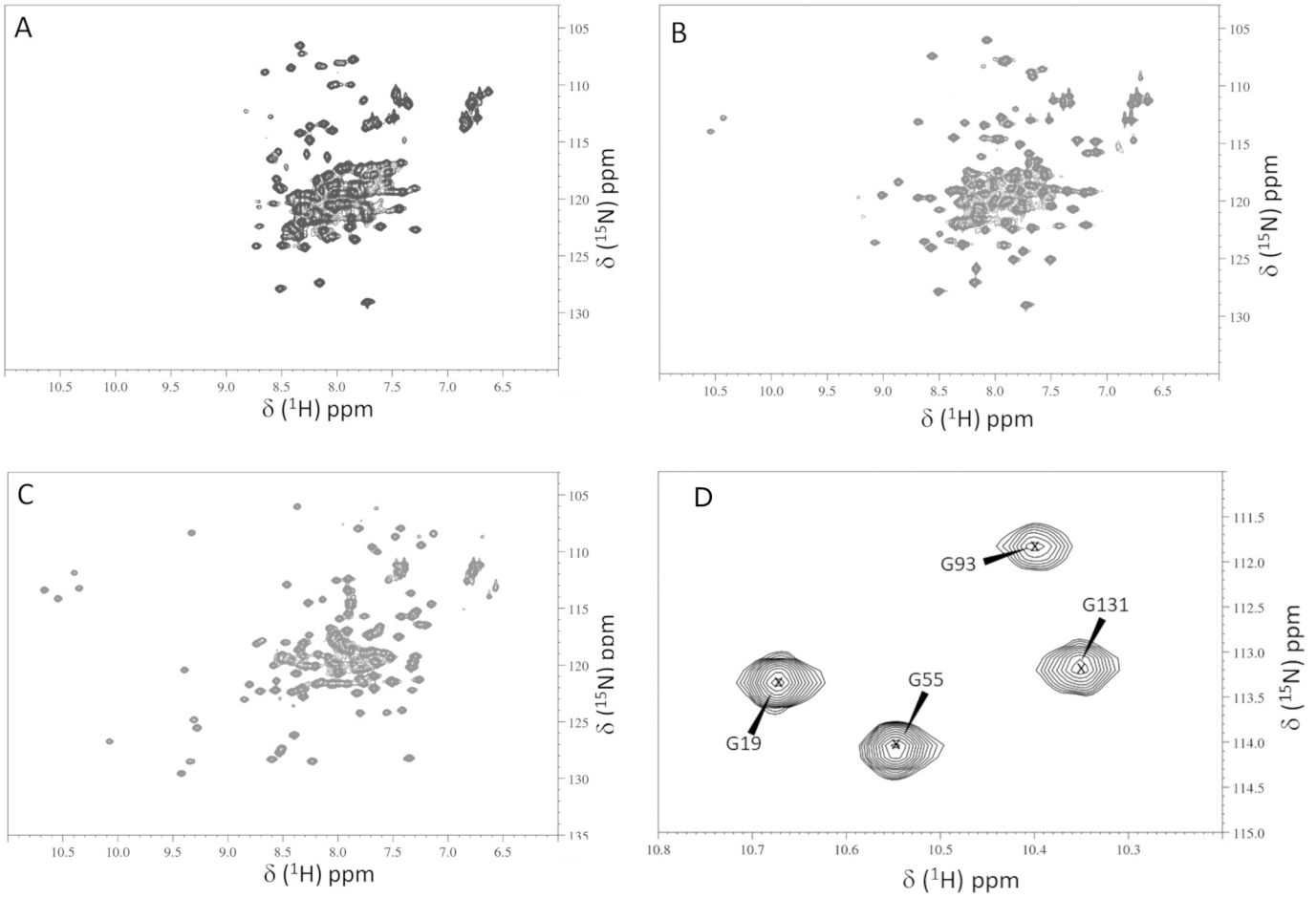

Fig. 1. Two-dimensional ^{1}H-^{15}N HSQC NMR spectra of apo- (A), Mg^{2+}-bound (B), Ca^{2+}-bound (C) ^{15}N-CML7 and zoom of the Gly_6 downfield peaks of Ca^{2+}-bound CML7 (D). The assignment of the Gly of the EF-hands is indicated by the position number of the residue. The spectra were recorded at 600 MHz at 298 K. All samples were at a protein concentration of 270 μM in 50 mM Tris-HCl, 50 mM KCl, 0.5 mM DTT, 7% D_2O pH 7.5.

pGREAT::eGFP; [38]) were mixed together before adding them to 100 μL MMg isolated protoplasts and then an equal amount of polyethylene glycol (PEG) solution (40% *v*/v PEG4000, 0.2 M D-Mannitol, 1 mM $CaCl_2$) was added, mixed gently and incubated at room temperature for 20 min. The protoplasts suspension was then diluted by adding a 4-fold volume of W5 to remove PEG. The supernatant was carefully removed after 3 min centrifugation at 100*g* and the transformed protoplasts resuspended in 1 mL W5 solution and maintained at 23 °C in the dark. Protoplasts were microscopically analyzed 16–24 h after transformation.

2.10. Confocal laser scanning microscopy

Confocal microscopy analysis was performed using a Nikon Eclipse Ti2 inverted microscope, equipped with a Nikon A1R+ laser scanning device (Nikon, http://www.nikon.com/products/microscope-solutions/lineup/confocal/a1/index.htm). EGFP and chlorophyll were excited with the 488 nm laser and the emission was collected at 500–550 nm and 663–738 nm, respectively. RFP was excited with the 561 nm laser and the emission was collected at 570–620 nm. The pinhole was set to 1.2 airy unit. Images were acquired by a CFI Plan Apo Lambda 60X Oil (N.A. 1.4) objective and were analyzed using Fiji software (https://fiji.sc).

2.11. Homology modelling and sequence analysis

The homology model of the CML7 from *A. thaliana* in the Ca^{2+}-bound form was generated using SWISS-MODEL Homology Modelling server (swissmodel.expasy.org) [39,40]. The template chosen for modelling procedure was the CaM from *Paramecium tetraurelia* (Protein Data Bank (PDB) entry: 1clm [41]) that shares with CML7 the higher sequence identity (42.0%) among proteins whose structures have been solved so far. The Global Model Quality Estimation (GMQE) index was 0.77, and the Qualitative Model Energy Analysis (QMEAN) potential scoring function was 1.21, indicating a good reliability for the obtained model. Sequence alignments were performed with NPS@ server [42]. Molecular graphics images were produced using the UCSF Chimera package from the Resource for Biocomputing, Visualization, and Informatics at the University of California, San Francisco (supported by NIH P41 RR-01081) (http://www.cgl.ucsf.edu/chimera). Molecular surface was coloured with the Coulombic Surface colouring (colouring parameters: μ = 4, thresholds ± 12 kcal mol^{-1} at 298 K) implemented in Chimera (http://www.cgl.ucsf.edu/chimera).

3. Results

3.1. CML7 production

CML7 from *A. thaliana* was successfully expressed as a recombinant protein in *E. coli* and purified to homogeneity by heat treatment and hydrophobic interaction chromatography; CML7 binds to a phenyl-sepharose column in the presence of Ca^{2+} and is released by the addition of EGTA (see Section 2.2). Ca^{2+}-dependent hydrophobic binding to phenyl-sepharose is typical of classic Ca^{2+} sensors, and thus represents

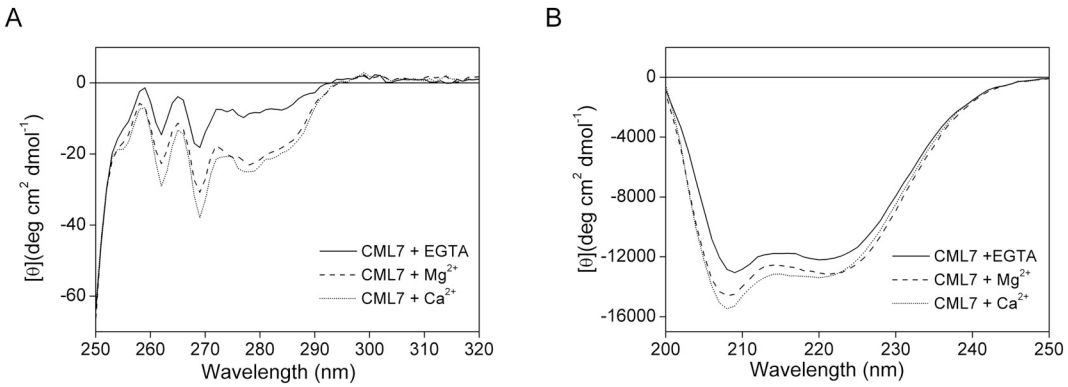

Fig. 2. Near and far UV CD spectra of CML7. (A) Near UV CD spectra of 100 μM CML7 and (B) far UV CD spectra of 12 μM CML7 after sequential addition of 1 mM EGTA (solid line), 2 mM $MgCl_2$ (dashed line) and 2 mM $CaCl_2$ (dotted line).

a first clue indicating that CML7 has Ca^{2+} sensor properties. Moreover, CML7 displayed a large electrophoretic mobility shift in the presence of Ca^{2+}, in both native and denaturing conditions (Supplementary Fig. S1), which is another characteristic of Ca^{2+} sensors. Both apo- and Ca^{2+}-bound CML7 show a single band on gel electrophoresis in the presence of DTT (Supplementary Fig. S1, lanes 1 and 2), while additional bands were present in the absence of DTT for both forms, independently of the presence of Ca^{2+} (Supplementary Fig. S1, lanes 3 and 4). This behavior is likely due to the presence of oligomers through formation of intermolecular disulphide bridges via Cys oxidation.

3.2. Apo-, Mg^{2+}- and Ca^{2+}-bound states of CML7 exist in distinct structural conformations

A hallmark of CaM and related Ca^{2+} sensors is the ability to experience a reversible conformational change upon Ca^{2+} binding that leads to the exposure of hydrophobic regions through which these proteins bind and regulate their downstream targets. Two-dimensional NMR spectra (^{1}H-^{15}N HSQC) of ^{15}N-labeled CML7 were collected to monitor conformational changes in CML7 resulting from Mg^{2+} and Ca^{2+} binding to the protein (Fig. 1). In each spectrum, the peaks are representative of protons in the main and side chain amides, and their dispersion is a good probe of protein conformation. As shown in Fig. 1, the apo-, Mg^{2+}- and Ca^{2+}-bound states of CML7 exist in distinct structural conformations. Easily observed in the ^{1}H-^{15}N HSQC spectra, upon addition of either Mg^{2+} or Ca^{2+} ions to the apo-protein a better dispersion of NMR signals was observed, and new peaks appeared, including downfield shifted peaks between 10 and 11 ppm in the ^{1}H dimension and 111–115 ppm in the ^{15}N dimension, which are indicative of metal binding in the EF-hand motifs. In particular, the ^{1}H-^{15}N HSQC spectra indicate that the Mg^{2+}-bound conformation of CML7 is separate from both its apo- and Ca^{2+}-bound states (Fig. 1). The broadening of the existing resonances line and the fewer number of peaks observed in the spectrum of Mg^{2+}-CML7, compared to that of the Ca^{2+}-CML7, suggest that Mg^{2+} and Ca^{2+} bind to CML7 with different affinities and that the Mg^{2+}-bound form of CML7 may still possess a degree of flexibility. Despite this partial conformational instability, the dispersion of resonances observed in the two-dimensional spectrum of Mg^{2+}-CML7 is distinct from the narrow range of ^{1}H chemical shifts observed in the apo-CML7 spectrum and favors a more folded conformation of the protein when bound to Mg^{2+}. The addition of Ca^{2+} to CML7 promoted a further change in chemical shifts that describes the transition between a closed apo conformation and an open Ca^{2+}-bound state, analogous to that observed with both mammalian and plant CaMs [8–10,13–15,43,44].

Many EF-hand proteins, including CML7, are characterized by a hydrogen bond network in metal-bound loops that causes the appearance of downfield-shifted peaks in the ^{1}H-^{15}N HSQC spectra, which belong to the backbone amides of glycine residues present at position 6 (Gly_6) of the EF-hands when bound to metal [14,15,43,45,46]. The extent of this downfield shift enables these resonances to act as indicators for the Ca^{2+}-bound state of a given EF-hand, providing indication on the stoichiometry of ion binding. The ^{1}H-^{15}N HSQC spectra of Ca^{2+}-bound CML7 showed four downfield shifted resonances (Fig. 1). Based on standard triple resonance NMR experiments acquired on ^{15}N,^{13}C-labeled CML7 in its Ca^{2+} bound state, we assigned the four resonances at positions 10.68, 10.55, 10.40 and 10.35 ppm (^{1}H dimension) to the Gly_6 of the EF-hands, Gly19 (EF-1), Gly55 (EF-2), Gly93 (EF-3), and Gly131 (EF-4), respectively (Fig. 1D). Thus, the presence of four low-field resonances corresponding to Gly_6 of the four EF-hands strongly suggests that CML7 can bind Ca^{2+} ions with a stoichiometry of 1:4 protein to metal ratio.

The ^{1}H-^{15}N HSQC spectral features of CML7 were consistent with our CD experiments. The near UV CD fingerprint of CML7, which reflects protein tertiary structure through local arrangements of aromatic residues, closely resembles that of CaM. Bands at 269 and 262 nm arising from Phe side chains are very well resolved with a broad minimum for Tyr at around 280 nm. No peaks corresponding to Trp residue are present as CML7 lacks Trp. Binding of Mg^{2+} to apo-CML7 produced significant changes in the near UV CD spectrum, with a decrease in the negative ellipticity both in the Phe and Tyr bands (Fig. 2A, dashed line). Addition of Ca^{2+} refined the spectrum, slightly increasing the signal intensity, consistently with further changes in the tertiary structure upon Ca^{2+} binding (Fig. 2A, dotted line). These results were supported by CD spectra in the far UV region which indicated CML7 to possess significant α-helical structure and characteristic negative ellipticity bands at 222 nm and 208 nm in both the apo- and metal-bound forms (Fig. 2B). Upon Ca^{2+} binding, CML7 showed a change of the spectrum characterized by an increase in intensity and variations in shape. These are visible as a change in the $\theta_{222}/\theta_{208}$ ratio (0.94 for apo-CML7 and 0.86 for Ca^{2+}-bound CML7), which could be ascribed mainly to helix reorientation within the tertiary structure, and not merely to a change in α-helical content [47,48].

CD data clearly indicated that both Ca^{2+} and Mg^{2+} ions induce conformational changes, affecting the secondary and tertiary structure of CML7. The metal binding also resulted in an increase of the thermal stability of the protein. Fig. 3A shows the thermal unfolding profiles of apo- and metal-bound CML7 obtained by following the CD signal at 222 nm as a function of temperature. In comparison to the sample containing CML7 and EGTA, the melting temperature (T_m) of CML7 with Mg^{2+} increased from 40.9 ± 0.8 °C to 60.0 ± 0.4 °C (Table 1). In the presence of Ca^{2+}, no estimate of T_m was possible as the denaturation curve increases monotonically with increasing temperature up to ~95 °C, and even at 95 °C the protein maintains a partially folded state. Along with this, the Ca^{2+}-bound form of CML7 was more stable against proteolysis by trypsin compared to the apo-form (Supplementary Fig.

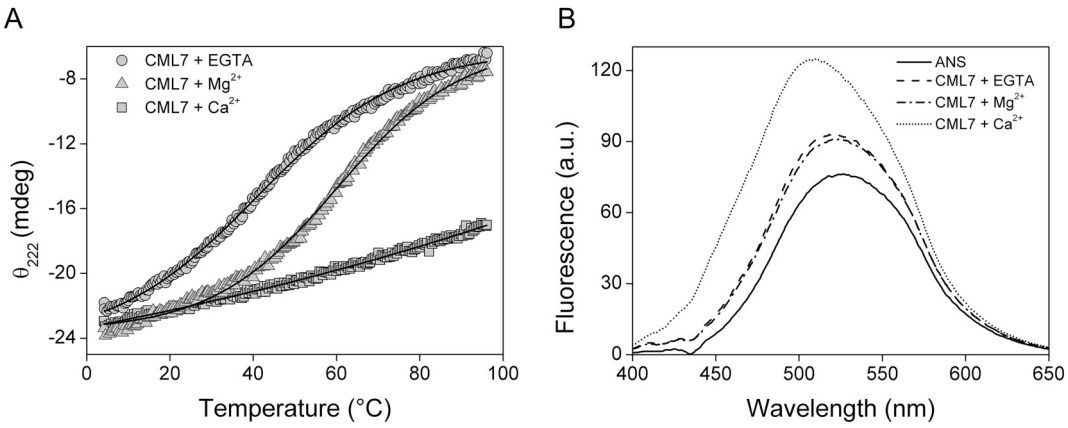

Fig. 3. CML7 thermal stability and ANS fluorescence. (A) Thermal denaturation profiles of 12 μM CML7 in the presence of 1 mM EGTA (circle), 2 mM $MgCl_2$ (triangle) and after addition of 2 mM $CaCl_2$ (square). (B) ANS fluorescence spectra of CML7 upon incubation with 2 mM EGTA (dashed line), 0.5 mM EGTA plus 5 mM $MgCl_2$ (dot dashed line) and 2 mM $CaCl_2$ (dotted line). The fluorescence spectrum of ANS alone is also shown (solid line).

Table 1
Analysis of ANS and CD thermal denaturation data for CML7.

	Blue shift (nm)[a]	F_{max}/F_{ref}[b]	Tm (°C)[c]
CML7 + EGTA	7 ± 1	1.2 ± 0.1	40.9 ± 0.8
CML7 + $MgCl_2$	6 ± 2	1.2 ± 0.1	60.0 ± 0.4
CML7 + $CaCl_2$	21 ± 2	1.6 ± 0.1	> 95

[a] Shift of the wavelength of maximum emission of CML7 + ANS mixture following excitation at 380 nm as compared to that of ANS alone.

[b] Ratio between maximal fluorescence emission of CML7 + ANS mixture and that of ANS alone.

[c] Melting temperature obtained by data fitting in thermal denaturation profiles.

S2).

This data suggests that the binding of Ca^{2+} or Mg^{2+} strongly stabilizes CML7 by leading to a rearrangement in both the secondary and the tertiary structures. However, for each metal the stabilized final conformation is distinct. Using the hydrophobic fluorescent probe ANS, we demonstrated that the binding of Ca^{2+} induces a domain opening in CML7 leading to the exposure of hydrophobic regions, whereas Mg^{2+} does not. As shown in Fig. 3B and Table 1, upon addition of Ca^{2+} to CML7 a blue-shift in the emission peak of ANS fluorescence (from 525 nm to 504 nm) was observed along with a ~2-fold increase in the maximal emission intensity, indicating that the hydrophobic regions of the recombinant CML7 were exposed to solvent, and therefore accessible to the ANS probe. On the contrary, the addition of Mg^{2+} to CML7 did not cause a significant change in the ANS fluorescence spectrum compared to that observed in the apo form. However, few variations in the emission spectra were observed for either apo-CML7 or Mg^{2+}-bound CML7 compared to the spectrum of ANS alone, suggesting that some hydrophobic exposure is present even in the absence of Ca^{2+} (Fig. 3B and Table 1). Thus, we showed that, in accordance with a putative function as a Ca^{2+} sensor, CML7 undergoes a large structural rearrangement leading to hydrophobic exposure only upon binding Ca^{2+}.

3.3. The C-lobe contains the higher affinity Ca^{2+} binding sites

We assessed Ca^{2+} binding to CML7 by ITC, starting from conditions of decalcified protein and buffer (Fig. 4). Data were fit using a sequential binding model with the stoichiometry of Ca^{2+} binding fixed to four (as deduced by NMR experiments) and following a procedure used previously for mammalian CaM and similar EF-hand containing Ca^{2+}-binding proteins [14,15,33,43,49–52]. The values obtained for the four macroscopic binding constants showed that the Ca^{2+} binding sites in CML7 are grouped into two pairs of different strength (Table 2): a first set of sites that comprises two high-affinity sites (K_{d1} = 0.9 ± 0.2 μM, K_{d2} = 0.5 ± 0.1 μM, respectively) and a second set that likely represents the binding of two Ca^{2+} ions with lower affinity (K_{d3} = 14.7 ± 0.8 μM, K_{d4} = 29.4 ± 4.7 μM). Ca^{2+} binding to CML7 followed an exothermic reaction, displaying a negative enthalpy change, which can be ascribed almost entirely to Ca^{2+}-induced conformational changes in the N- and C-terminal domains of CML7, since the ΔH associated with Ca^{2+} binding/desolvation can be approximated to be zero [43,49].

To learn more about the pathways of Ca^{2+} binding to CML7, Ca^{2+} was titrated into a solution of apo-CML7 and two-dimensional ^{1}H-^{15}N HSQC spectra were recorded at each step. As shown in Fig. 5A, the Gly_6 peaks for the C-terminal lobe (Gly93 and Gly131) appeared simultaneously at Ca^{2+}: protein ratios lower than those of the N-terminal Gly_6 (Gly19 and Gly55) which develop together only at higher Ca^{2+}: protein ratios. These observations indicate that the high affinity sites are located in the C-lobe of CML7 and allowed us to assign the dissociation constants determined from ITC K_{d1} and K_{d2} to the C-terminal domain (higher affinity Ca^{2+}-binding sites), and K_{d3} and K_{d4} to the N-terminal EF-hands (lower affinity Ca^{2+}-binding sites).

The paired nature of these plant CML7 EF-hands and the fact that two of the sites have higher Ca^{2+} affinity than the other two enabled us to estimate the cooperativity within each EF-hand pair. The cooperativity in a two-site system (EF-hand pair) can be quantified in terms of free energy, with the term $-\Delta\Delta G$ reflecting the increase in affinity of the second EF-hand as a result of Ca^{2+} binding to the first [53,54]. If the affinity for the second ion is greater than the first, this term is positive, indicating positive cooperativity. As shown in Supplementary Table S1, each pair of CML7 EF-hands displayed positive cooperativity. Thus, we can conclude that the two sites of the C-terminal domain in CML7 bind Ca^{2+} most strongly in a cooperative manner.

We next investigated the influence of Mg^{2+} on the Ca^{2+}-binding thermodynamic parameters as well as association constants of CML7 by ITC. Ca^{2+} titrations were performed upon incubation of CML7 with 10 mM $MgCl_2$ (Fig. 4B, Table 2, Supplementary Table S1). Although the four EF-hand Ca^{2+}-binding sites still bind Ca^{2+} with positive cooperativity, the presence of 10 mM Mg^{2+} slightly decreased the Ca^{2+} association constants of sites 1 and 2 (~up to 6-fold), while it did not significantly modify the Ca^{2+} association constants of the lower affinity sites (sites 3 and 4) of CML7. In the presence of Mg^{2+}, the Ca^{2+}-binding preference of the EF-hands of CML7 remains unchanged, and the C-terminal sites are occupied before the N-terminal sites, as observed in NMR titration experiments (data not shown). Importantly, Ca^{2+} addition to Mg^{2+}-bound CML7 leads to the disappearance of the peaks associated with Mg^{2+} bound form in ^{1}H-^{15}N HSQC spectrum and the

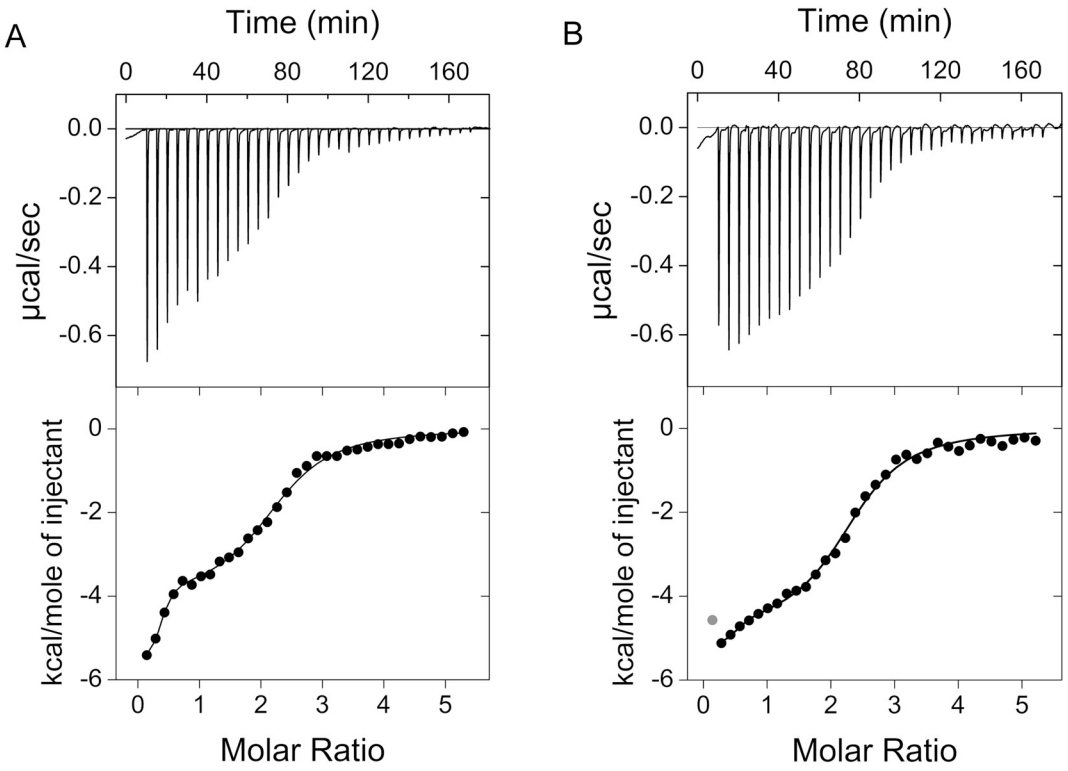

Fig. 4. ITC analysis of the Ca^{2+} binding to apo- and Mg^{2+}-bound CML7. Representative raw trace (top) of the calorimetric titration of $CaCl_2$ into 200 µM apo-CML7 (A) and 200 µM CML7 pre-incubated with 10 mM $MgCl_2$ (B), and integrated binding isotherm (bottom). Curve fitting was performed using a four-site sequential binding model. The ligand dilution blank experiments (Ca^{2+} ions titrated into buffer only) were subtracted from the binding isotherm obtained in the presence of protein.

Table 2
Thermodynamic parameters for Ca^{2+} binding to CML7. The mean values from triplicate experiments and SEM using at least two different CML7 preparations are presented.

	No Mg^{2+}			+10 mM Mg^{2+}		
	K_a (M^{-1})	K_d (µM)	ΔH (kcal mol^{-1})	K_a (M^{-1})	K_d (µM)	ΔH (kcal mol^{-1})
Site 1	1.1E6 ± 2.9E5	0.9 ± 0.2	−6.6E3 ± 0.8E3	2.6E5 ± 6.3E4	3.8 ± 0.9	−5.9E3 ± 0.9E3
Site 2	2.2E6 ± 4.1E5	0.5 ± 0.1	−1.6E3 ± 0.4E3	3.2E5 ± 6.2E4	3.1 ± 0.6	−1.9E3 ± 0.3E3
Site 3	6.8E4 ± 3.9E3	14.7 ± 0.8	−3.1E3 ± 0.7E3	4.9E4 ± 7.3E3	20.4 ± 3.0	−2.6E3 ± 0.6E3
Site 4	3.4E4 ± 5.4E3	29.4 ± 4.7	−1.5E3 ± 0.4E3	2.6E4 ± 8.4E3	38.5 ± 6.9	−0.8E3 ± 0.1E3

Sites 1 and 2 can be assigned to the C-terminal lobe and sites 3 and 4 to the N-terminal lobe. The domain-specific assignment is based on NMR analysis (see text for explanation).

concomitant appearance of the peaks characteristic of the Ca^{2+}-bound CML7; the resulting spectrum is nearly superimposable with that of Ca^{2+}-CML7 (Figs. 1C, 5). This provides evidence of Mg^{2+} displacement by Ca^{2+}, and that CML7 attains the same conformation after binding Ca^{2+}, in both the presence and absence of Mg^{2+}.

3.4. Melittin binds to CML7

Melittin (GIGAVLKVLTTGLPALISWIKRKRQQ) is an amphipathic model peptide that is widely used to study the interaction of downstream targets with proteins of the CaM family. It is well-known that melittin interacts with Ca^{2+}-saturated bovine CaM to form a 1:1 complex with nanomolar affinity [55], assuming an α-helix conformation upon binding [56]. In an effort to demonstrate that CML7 behaves as a member of CaM family towards the interaction of targets and since the CML7 physiological target in plants has not been identified, we examined CML7 for interaction with melittin. A canonical plant CaM (AtCaM1 from *A. thaliana*) was used as a positive control in our experiments.

First, we monitored the interaction of CML7 or AtCaM1 with melittin in the presence of increasing amounts of the peptide by native PAGE (Fig. 6A). Nondenaturing gel band shift electrophoresis directly confirmed that melittin forms a 1:1 complex with AtCaM1 in the presence of Ca^{2+}, but not in its absence (i.e. in the presence of 5 mM EGTA (Fig. 6A)). The peptide also forms a complex with CML7 in the presence of Ca^{2+}. Upon addition of melittin, the single band reflecting pure CML7 disappeared and a new protein band of lower mobility appeared, indicating the formation of a new complex. At 1:1 protein:peptide ratio, almost all the free CML7 disappeared, suggesting the 1:1 formation of a peptide/CML7 complex. At higher concentrations of melittin, a smearing of the band representing the complex was observed, likely indicating that additional binding occurs (up to 4 mol of melittin/mol of CML7).

Formation of CML7/melittin and AtCaM1/melittin complexes was also studied by fluorescence spectroscopy. Both CML7 and AtCaM1 do not have any Trp residues, while melittin possesses one Trp (Trp19).

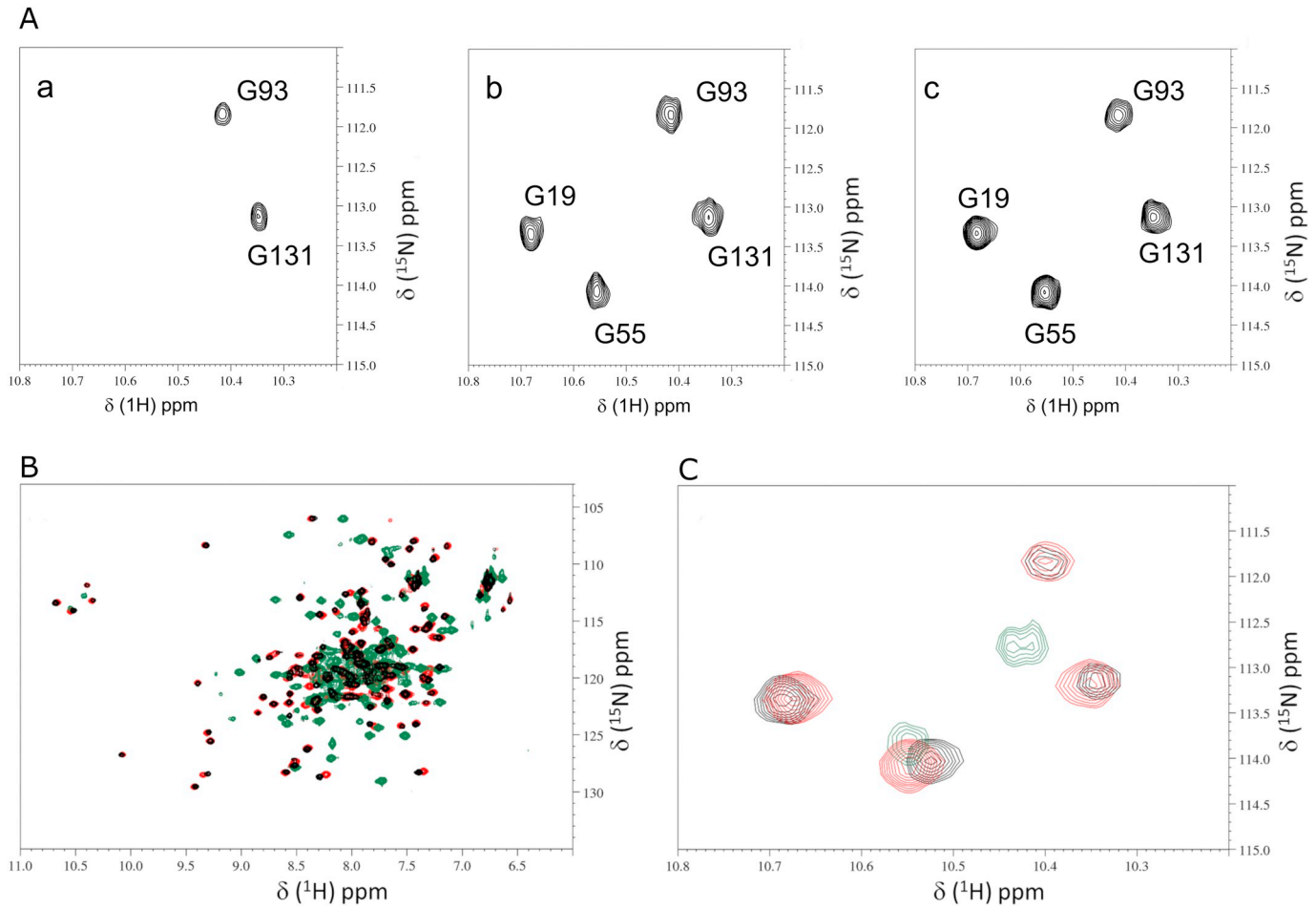

Fig. 5. NMR analysis of the Ca^{2+} binding to apo- and Mg^{2+}-bound CML7. (A) Downfield region of selected ^{1}H-^{15}N HSQC NMR spectra of CML7 recorded as a function of increasing Ca^{2+} concentration. The molar ratio of Ca^{2+}: protein was 2 (a), 4.5 (b), 10 (c). (B) Superimposition of ^{1}H-^{15}N HSQC spectra recorded on ^{15}N-CML7 after addition of 5 mM $CaCl_2$ (red), 20 mM $MgCl_2$ (green), or 20 mM $MgCl_2$ + 20 mM $CaCl_2$ (black). (C) Zoom of the Gly downfield peaks. The spectra were recorded at 600 MHz and 298 K. All samples were at protein concentration of 270 μM in 50 mM Tris, 50 mM KCl, 0.5 mM DTT, 7% D_2O pH 7.5.

This intrinsic fluorophore is a useful probe to monitor binding of the peptide to the protein since, upon complex formation it usually experiences changes in its spectral properties (maximum emission wavelength and/or fluorescence intensity). As expected for a solvent exposed Trp residue, for melittin alone, the maximum fluorescence emission wavelength is 354 nm. Upon the addition of $CaCl_2$ to the melittin solution, no changes in the fluorescence spectrum were observed, while the fluorescence was blue shifted to 339 nm and 338 upon binding to AtCaM1 and CML7, respectively (in the presence of saturating concentrations of Ca^{2+}) (Fig. 6B). This large blue shift is indicative of an augmented hydrophobicity of the Trp environment, suggesting that interaction between proteins and melittin occurs. The weaker intensity of the Trp fluorescence emission when melittin is bound to CML7 compared to AtCaM1 may be due to increased quenching either by the surrounding amino acid side chains or from a greater exposure to solvent. The microenvironment of the Trp residue of melittin could be perturbed in a different way in the two complexes. However, it might also suggest that the Trp is less rigidly held in the binding pocket, therefore we cannot exclude the presence of conformational changes which could potentially alter the fluorescence properties of melittin in a different manner in the two complexes.

To estimate the apparent affinity between proteins and melittin, titration experiments in Trp fluorescence were performed (Fig. 6C). Our data showed that, in the presence of Ca^{2+}, AtCaM1 binds melittin with high affinity (K_d of 8 ± 2 nM) and with 1:1 stoichiometry, in line with previously reported data for bovine CaM/melittin interaction [55]. Binding of melittin to Ca^{2+}-bound CML7 also occurs with high affinity (K_d of 0.3 ± 0.1 μM), even if lower compared to AtCaM1.

Furthermore, we acquired CD spectra to examine whether binding of melittin to AtCaM1 or CML7 is associated with changes in secondary structure. As shown in Fig. 6D and 6E, CD signals of both AtCaM1 and CML7 were increased following the addition of melittin. In aqueous solution, free melittin has a small α-helical content. The observation of α-helix formation is not uncommon in monomeric peptides that are 20–25 residues in length [57,58]. The far UV CD spectrum of AtCaM1 and CML7 showed two minima peaks at 208 and 222 nm, which is typical of a protein with a significant α-helical content, as described above [33,59]. Addition of equimolar melittin to AtCaM1 or CML7 yielded a spectrum that was more negative than the sum of each taken separately, suggesting that the α-helical content of the Ca^{2+}-protein/peptide complex increases (Fig. 6D, E). The higher value of CD signal observed is attributable to induced helicity in melittin, since Ca^{2+}-CaM itself does not gain secondary structure following binding to target peptide [60,61]. Moreover, in the case of AtCaM1, the shape of the spectrum representing the complex was also different from the individual components. In the presence of melittin and Ca^{2+}, the $\theta_{222}/\theta_{208}$ ratio for AtCaM1 approaches the value of ~1.08 observed for coiled-coil motifs. Thus, it is possible that a tight interaction between α-helices, which in certain regions may coil together, occurs when AtCaM1 binds melittin.

Importantly, in the presence of EGTA, CD spectra were characterized by only a modest change upon addition of melittin to CML7

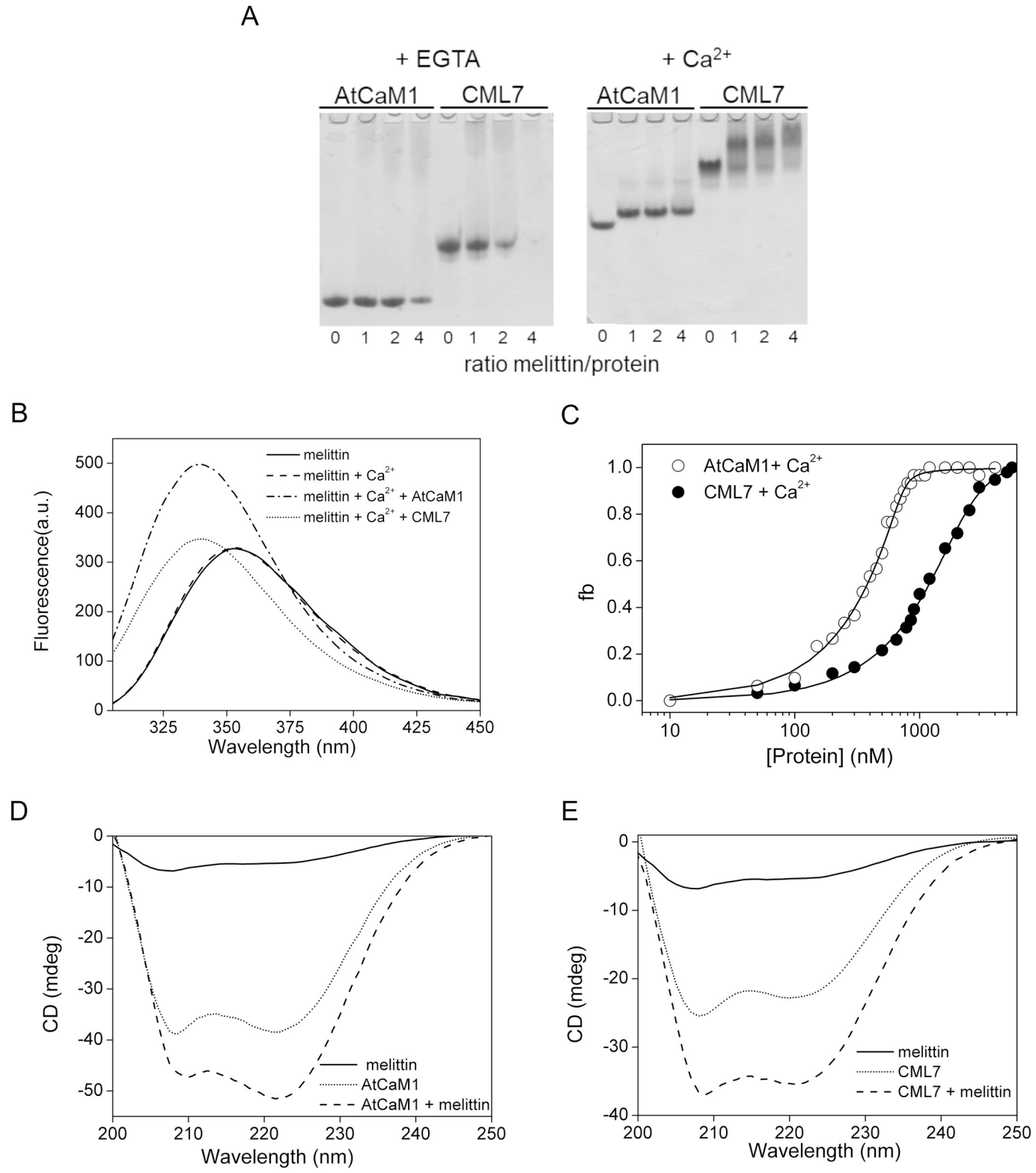

Fig. 6. Interaction of melittin with AtCaM1 and CML7. (A) Native PAGE in the presence of $CaCl_2$ or EGTA. (B) Complex formation monitored by Trp fluorescence. Emission spectra, recorded in the presence of $CaCl_2$, of melittin (dashed line), melittin/AtCaM1 (dash dotted line) and melittin/CML7 complex (dotted line). The spectrum of melittin before addition of $CaCl_2$ (solid line) is also shown. (C) Fluorescence titration of AtCaM1 (open circles) or CML7 (filled circles) with melittin in the presence of $CaCl_2$. The K_d value is determined by fitting the fraction bound (fb) to Eq. (1). (D–E) Far UV CD spectra changes in secondary structure for AtCaM1/melittin (D) and CML7/melittin complex (E) in the presence of $CaCl_2$. Melittin alone (solid line), AtCaM1 or CML7 alone (dotted line), and protein/peptide complex at 1:1 molar ratio (dashed line).

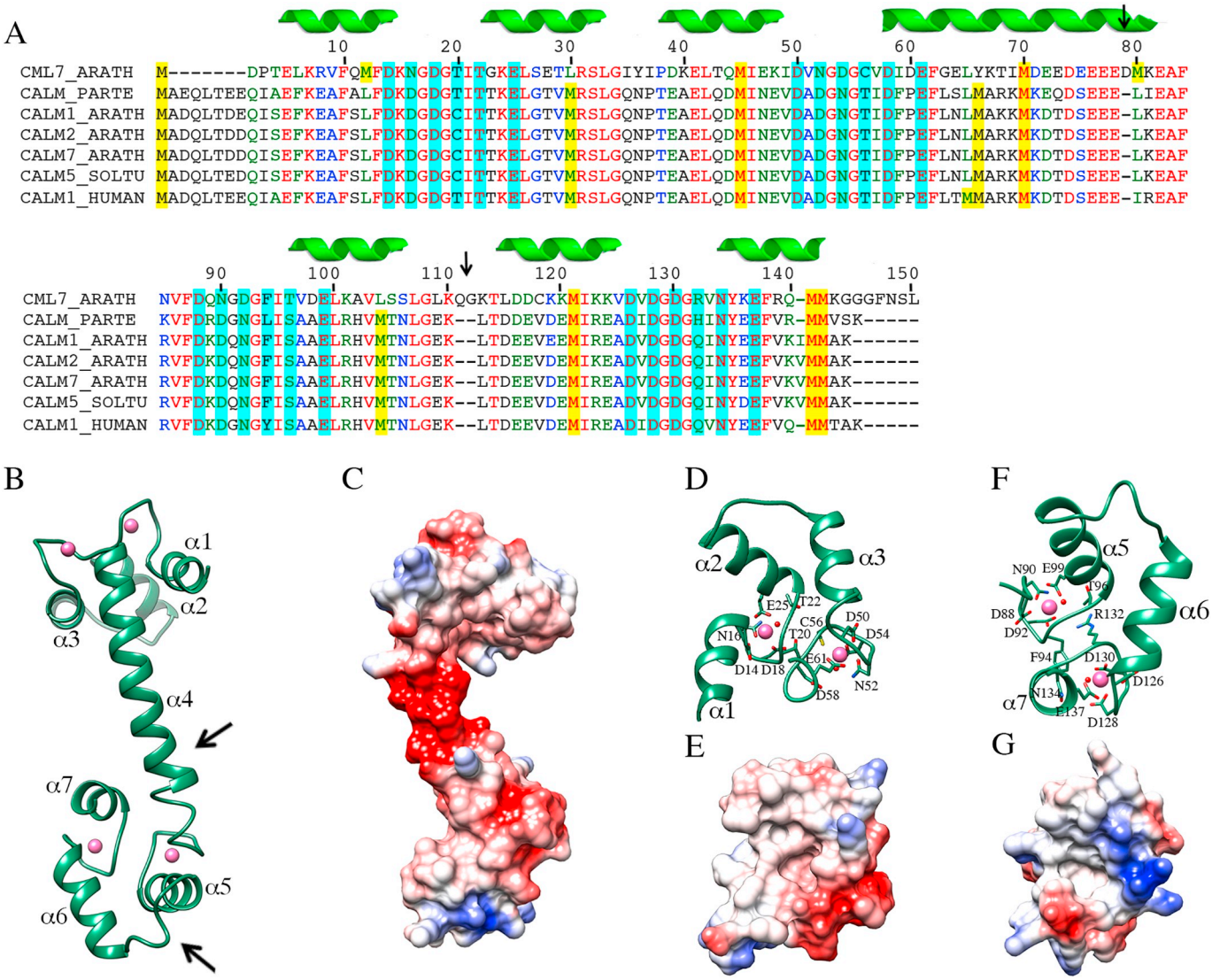

Fig. 7. Sequence alignment and molecular modelling of CML7. (A) Sequence alignment of CML7_ARATH (CML7 from *A. thaliana*; Uniprot: Q9LNE7), CALM_PARTE (CaM from *P. tetraurelia*; Uniprot: P07463), CALM1_ARATH (CaM1 from *A. thaliana;* Uniprot: P0DH95), CALM2_ARATH (CaM2 from *A. thaliana;* Uniprot: P0DH97), CALM7_ARATH (CaM7 from *A. thaliana;* Uniprot: P59220), CALM5_SOLTU (CaM5 from *S. tuberosum;* Uniprot: Q7DMN9), CALM1_HUMAN (CaM1 from *H. sapiens;* Uniprot: P0DP23); residues involved in Ca^{2+} coordination are highlighted in light blue, Met in yellow; black arrows represent amino acid insertion in the CML7 sequence. Numbering and secondary structure elements assignments are highlighted for CML7. (B) Cartoon representation of the CML7 molecular modelling; Ca^{2+} is represented as a pink sphere; arrows represent region of amino acid insertion in the CML7 sequence. (C) Coulombing surface colouring of the CML7 molecular surface. (D–F) Close view of the N-lobe and the C-lobe respectively. Residues involved in Ca^{2+} coordination are represented in stick, water molecules (red spheres) were transferred from the template (E–G) Coulombing surface coloring of the CML7 N-lobe and the C-lobe.

(Supplementary Fig. S3), suggesting that the interaction takes place mainly in the presence of Ca^{2+}.

Our results showed that CML7 has a high affinity interaction with melittin, a model CaM interacting peptide, in a Ca^{2+}-dependent manner. Therefore, we can envisage that CML7 may be involved in Ca^{2+} mediated protein-protein interactions even if its physiological partner/s is still unidentified.

3.5. CML7 sequence analysis and homology model

A homology model of the CML7 from *A. thaliana* in the Ca^{2+} bound form was generated using the structure of the CaM from *Paramecium tetraurelia* (PDB entry: 1clm [41]) as template. The model assumes the dumbbell-like structure typical of CaM proteins formed by two structurally similar globular domains (the N-term lobe and the C-term lobe), containing a pair of Ca^{2+}-binding motifs connected by a central α-helix (Fig. 7B, C). It was recently reported that while the conformation of animal and *P. tetraurelia* CaM proteins are very similar, CaM6 from potato [62] and CaM7 from *A. thaliana* [63] show a different orientation of the central helix. The central linker connecting the two globular domains has been described as “magical” because it is highly flexible, allowing CaM to interact with a wide range of targets in a remarkable variety of conformations [64–66]. For this reason, while the CML7 model can be considered highly accurate in the Ca^{2+} binding domains, the region corresponding to the central helix may be less accurate. Moreover, CML7 has an amino acid insertion (Asp79) in the C-terminal end of the central helix (Fig. 7A, B) that may lead the linker to adopt different orientations compared to typical CaMs.

The Ca^{2+} binding site is composed of 12 residues in which positions 1, 3, 5, 7, 9 and 12 are occupied by residues that, together with a water molecule, contribute to Ca^{2+} coordination. Among them, residues in positions 1, 3, 5, and 12 participate in Ca^{2+} binding through side chain oxygen, residue in position 7 with main chain oxygen while residue in position 9 coordinates a water molecule (Fig. 7A, D, F) [26]. Analysis of

the primary structure of CML7 showed that all the four EF-hands in CML7 resemble those found in CaM proteins, especially in the positions devoted to Ca^{2+} binding (Fig. 7A), with minor differences. In the EF-hand 1, position 3, which is usually occupied by an Asp residue, is replaced by an Asn in CML7 (Fig. 7A). This conservative substitution is also present in other CMLs from *A. thaliana* belonging to the VII subgroup in the classification performed by Zhu [24], with the only exception of CML6 (Supplementary Fig. S4). EF-hand 2 of CML7 shows an Asp to Asn substitution in position 3, while position 5 (in which an Asn is usually present) is occupied by an Asp residue. Interestingly, EF-hand 2 is less conserved in the CMLs belonging to subgroup VII and appears to be not functional in CML42, CML43, and CML44 (Supplementary Fig. S4) [9,10,67]. Similarly to EF-hand 2 of CML7, also in EF-hand 3 Asp to Asn substitutions in positions 3 and 5 are present. The residues responsible for Ca^{2+} coordination are fully conserved in EF-hand 4. Interestingly, a two-residue insertion is present in the loop connecting EF-hand 3 and EF-hand 4 and it seems to be a general feature in the CML proteins belonging to subgroup VII (Supplementary Fig. S4).

In analogy to what reported for CaMs, it is likely that the binding of Ca^{2+} to each globular domain in CML7 changes the inter-helical angles in the EF-hand motifs, inducing exposure of hydrophobic sites that favors the interactions with downstream partners. As shown in Figs. 7E and G, the Coulombic surface of both N-terminal and C-terminal lobes of the model of CML7 in the Ca^{2+}-bound form revealed the presence of hydrophobic patches in which Met residues likely play a key role in the interaction with targets [68]. CML7 primary sequence contains eight Met residues; two of them are located in the N-lobe (Met12 and Met45), two in the central region (Met70 and Met80), and three in the C-lobe (Met121, Met141 and Met142). Only five of them are conserved in other CaMs (Fig. 7A). In addition to the exposure of hydrophobic residues upon Ca^{2+} binding, the ability of CaM to recognize different interacting molecules is assured by the presence of the helix [68,69]. In CML7, this helix appears to contain a negatively charged region that is longer than that present in CaM proteins (Fig. 7A, C). This region is quite variable among CMLs belonging to subgroup VII (Supplementary Fig. S4), and this diversity may contribute to different modes of target recognition and/or binding topology that distinguish CMLs from one another.

3.6. CML7 is localized in the cytoplasm

Protein localization is a necessary step if we aim to understand the function of CML7 in a physiological context and examine functional redundancy between CaM and CML isoforms. To determine the subcellular localization of CML7 in plant cells, we fused the RFP at the C-terminus end of CML7 and placed it under the control of the CaMV35S promoter. *A. thaliana* protoplasts cotransformed with the CML7-RFP fusion and the free EGFP showed green fluorescence with typical cytoplasmic localization (Fig. 8A). The red fluorescence from the CML7-RFP fusion was also restricted to cytoplasm (Fig. 8B), perfectly overlapping with the green fluorescence (Fig. 8E).

4. Discussion

Ca^{2+} has a central role in adaptive developmental and stress response programs in plants, regulating many important physiological processes. A number of abiotic and biotic stimuli elicit specific Ca^{2+} signals that usually occur via changes in cytosolic free Ca^{2+} concentration, and the shape of these Ca^{2+} signals is believed to specify the nature of the response [21,22]. The mechanisms by which changes in intracellular Ca^{2+} concentration can lead to diverse responses is a topic of widespread interest among plant biologists that has recently focused on the roles of CMLs as specialized Ca^{2+} sensors [20–22,70,71]. Importantly, the plant CML protein family is revealing its diversification among Ca^{2+}-binding proteins with respect to CaM [12,20–22,70–73].

There are 50 isoforms of CML in *A. thaliana*, and characterization of the different isoforms is essential to understand their functional significance. To this end, we have recently described the ion and target binding properties of several *A. thaliana* CMLs including CML14, CML19, and CML36 [8,14,15]. This investigation reports on the Ca^{2+} and Mg^{2+} sensing properties of CML7, as well as on metal induced conformational changes and binding to the model target peptide melittin.

Our results provide significant information regarding modulation of the structure of CML7 in the presence of saturating concentrations of Ca^{2+}. In the absence of Ca^{2+} ions, the CD spectrum shows extensive helical content, while ANS fluorescence suggests that the protein has a closed conformation and no or only limited exposure of hydrophobic surfaces. The ^{1}H-^{15}N HSQC spectrum is characterized by broad peaks, indicating conformational heterogeneity in the absence of Ca^{2+}. Under saturating Ca^{2+}conditions, transition between the heterogeneous closed conformation and the open conformation took place. Ca^{2+}-dependent exposure of hydrophobic regions as measured by ANS fluorescence, Ca^{2+}-dependent interaction of CML7 with hydrophobic phenyl-Sepharose, and increased mobility in electrophoresis in the presence of Ca^{2+}, collectively corroborated the significant Ca^{2+}-induced conformational change in CML7.

Moreover, molecular modelling of CML7 was performed in the Ca^{2+}-bound form. Our model suggests that the overall structure in CML7 is well conserved and assumes the dumbbell-like structure typical of CaM proteins, in which the N-lobe and C-lobe are devoted to Ca^{2+} binding through conserved or conservatively mutated residues. CML7 possesses four EF-hand motifs and the ability of all of them to bind Ca^{2+} was confirmed by the appearance in the NMR spectrum of Ca^{2+}-bound CML7 of four downfield-shifted resonances, which belong to the conserved Gly residues at position 6 of Ca^{2+}-occupied EF-hands. This stoichiometry was further supported by ITC analysis and by both amino acid sequence predictions and inspection of the CML7 model generated *in silico*. According to the ITC and NMR results, CML7 was shown to possess two high affinity Ca^{2+} sites in the C-lobe and two weaker sites

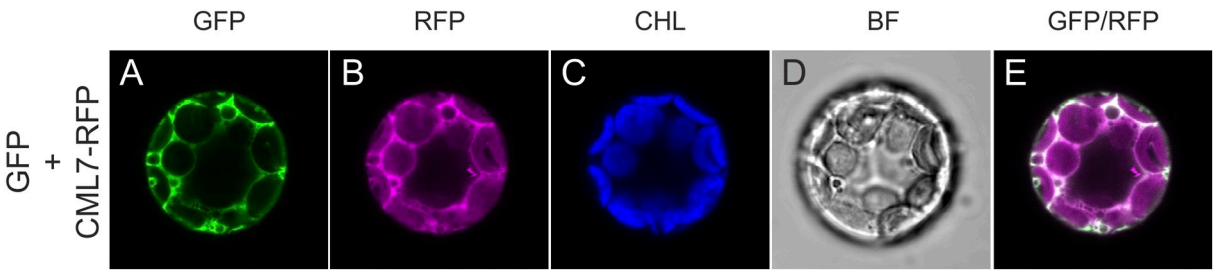

Fig. 8. Subcellular localization of CML7-RFP in *A. thaliana* mesophyll protoplasts. The CML7-RFP fusion protein was transiently coexpressed in protoplasts with free EGFP. Fluorescence was analyzed by confocal microscopy. (A) EGFP fluorescence (green) from a single focal plane of a representative protoplast. (B) RPF fluorescence (magenta) from the same protoplast as shown in (A). (C) Chlorophyll autofluorescence of chloroplasts. (D) Bright field image. (E) Overlay image of A and B.

in the N-lobe. This high/moderate Ca^{2+} affinity appears to be an emerging pattern in CMLs [12–14], and a wide range of Ca^{2+} affinity (nM-μM range) has been determined for this class of Ca^{2+} sensors [9,10,13,15]. The growing idea is that CMLs might possess different Ca^{2+} binding affinities to specifically sense a broad range of cytosolic free Ca^{2+} variations, being thus key players in Ca^{2+} signaling transduction. Along with this, the apparent affinity for Ca^{2+} for most CMLs differs considerably from the universal Ca^{2+} sensor CaM [9,10,13,15,33,43]. Importantly, positive cooperativity of Ca^{2+} binding is observed within each globular domain of CML7, in line with the paired nature of these plant CML7 EF-hands, and as frequently observed in EF-hand containing proteins [26,43,54,74].

We also studied the effect of Mg^{2+} on the binding of Ca^{2+} and the conformation of CML7. The interaction between Mg^{2+} and CML7 is crucial for understanding how CML7 specifically responds to micromolar variations in free cytosolic Ca^{2+} concentrations in the presence of ~1000-fold excess of the chemically similar Mg^{2+} ions. Ca^{2+} affinities of CML7 decreased by ~4–6-fold for C-terminal sites and ~1.3-fold for N-terminal sites when assessed in the presence of Mg^{2+}. Importantly, the order of Ca^{2+} binding to CML7 remained the same as that in the absence of Mg^{2+}, and similar positive cooperativity was also observed. The modest effect of Mg^{2+} on Ca^{2+} affinity of CML7, which is similar to the Mg^{2+}-based change in Ca^{2+} affinity seen for mammalian CaM [49], likely allows the EF-hands of CML7 to be classified as Ca^{2+}-specific sites [26]. The effect of Mg^{2+} on Ca^{2+} binding is still controversial and competition or allosteric effects of Mg^{2+} with respect to Ca^{2+} binding have been suggested [26,49,75,76]. Moreover, the presence of auxiliary Mg^{2+} binding sites distinct from the EF-hand Ca^{2+} binding sites in CaM has been proposed [44]. NMR spectra of Mg^{2+}-CML7 showed two downfield shifted Gly_6 resonances, pointing to the Mg^{2+} binding sites being located within the EF-loop structure. However, only the comparison of the crystal structure of Mg^{2+}-bound CML7 with the Ca^{2+}-bound CML7 could provide more insight into this aspect.

Owing to the excess Mg^{2+} concentration in the resting cell, many Ca^{2+}-specific EF-hands have enough affinity for this cation to be partially or even fully saturated with Mg^{2+} [26,77]. The crucial factor for efficient Ca^{2+} signaling is the difference in the resulting metal-bound protein conformation. Binding of Mg^{2+} to apo-CML7 induced changes in the secondary structure similar to those induced by Ca^{2+}. Moreover, both Ca^{2+} and Mg^{2+} stabilize CML7, as reflected in a large increase in the unfolding temperature. However, the Mg^{2+}-bound conformation of CML7 differs from the Ca^{2+}-bound form of the protein, as observed in NMR spectra, and CML7 does not experience a marked increase in surface hydrophobicity in the presence of Mg^{2+}, as demonstrated by the ANS data. This suggests that the Mg^{2+}-bound protein and the Mg^{2+}-bound loops likely remain in a "closed" conformation, analogously to that seen with Mg^{2+}-bound mammalian CaM [46], and therefore Mg^{2+} is not predicted to replace Ca^{2+} in hydrophobic-dependent target interaction. Consistent with this, the bidimensional NMR spectrum of Ca^{2+}-saturated CML7 in the presence of Mg^{2+} is essentially identical to that of the Mg^{2+}-free, Ca^{2+}-bound protein, indicating that Ca^{2+}-saturated CML7 has the same three-dimensional conformation both in the absence and in the presence of excess Mg^{2+}.

Overall, the results obtained indicate that CML7 belongs to the group of classical Ca^{2+} sensors instead of Ca^{2+}-buffering proteins, which experience only minor structural variations and bind very tightly to Ca^{2+} [26]. Working as a Ca^{2+} sensor, CML7 is therefore expected to interact with and/or regulate specific target proteins. Inspection of the coulombic surface of CML7 in our *in silico* model indicates that the inner surfaces of the N- and C-term lobes contain Met-rich hydrophobic patches, while acidic clusters are present in the linker region. The presence of these hydrophobic and acidic regions is likely instrumental for interaction with target proteins and suggests the necessity for preserving the contact sites with the effector molecule with respect to CaM. CaM-binding sites are usually positively charged, amphiphilic α-helical peptides with bulky hydrophobic anchor residues (e.g. Trp) that are often located at one or both ends of the helix [78]. Thus, CaM binding to its targets usually involves both hydrophobic and electrostatic interactions [60,61]. Melittin, a small peptide of 26 residues, is widely used to study protein–peptide interactions in Ca^{2+}-binding proteins, including CaM, and can provide insight into target recognition mode of CaM [55,79,80]. Earlier studies of the Ca^{2+}-CaM/melittin complex have shown that the binding of melittin to bovine CaM occurs with high affinity (K_d in nanomolar range) and in a parallel orientation, meaning that the N- and C-terminal regions of the peptide are associated with the N- and C-term domains of the protein, respectively [56,79]. Herein, by nondenaturing-PAGE, CD spectroscopy, and steady state Trp fluorescence we showed that plant CaMs (i.e., CaM1 from *A. thaliana*) are also able to bind melittin peptide with a 1:1 stoichiometry and very high affinity, in agreement with the previously reported bovine Ca^{2+}-CaM/melittin interaction [55]. Importantly, we further demonstrated that CML7 binds the natural peptide melittin in the presence of Ca^{2+}. According to our results, the melittin/CML7 interaction has a 1:1 stoichiometry with a K_d of 0.3 ± 0.1 μM. Binding of melittin to Ca^{2+}-AtCaM1 and Ca^{2+}-CML7 occurred in an α-helical conformation, and the interaction involved the Trp residue of the peptide which becomes solvent shielded.

The binding of melittin definitely places CML7 in the group of Ca^{2+} sensors, but more insightful information will require identification and examination of the formation of complexes between CML7 and peptides that arise from its physiological targets. Moreover, although important clues can be obtained by the analysis of CML complexes with short target peptides, these complexes do not always perfectly reflect the biophysical and structural properties of the full-length protein. Therefore, in the absence of physiologically significant functional information, the structural and biochemical data should be interpreted with caution.

An involvement of CML7 in root development has been proposed [27], even if the downstream targets of CML7 have not yet been identified. Despite the large number of molecular interactions that take place with members of the CaM superfamily, specific differences in the structure of physiological targets are likely to ensure specificity of interactions. Indeed, there may be large differences in target binding among CMLs, and ultimately each CML/target interaction must be verified separately. However, it is worth noting that the structural properties and the mechanism of action of CML7 and AtCaM1, as predicted from our results, seem to be very similar. Thus, it is unclear how they can have non-overlapping physiological functions. Clearly, for Ca^{2+} sensors it is crucial to consider the Ca^{2+} binding properties in connection with the target. Moreover, factors other than Ca^{2+} binding, such as relative abundance of Ca^{2+} sensor and target, tissue expression, and cellular localization as well as phosphorylation may have significant implications for target regulation mechanism. Subcellular localization is an important attribute of protein function, since, usually, Ca^{2+} sensors and their interacting targets colocalize. CML7 was empirically demonstrated to be cytosolic, therefore providing further clues into understanding of the Ca^{2+}/CML7 signal transduction pathway. However, only the identification of the physiological targets of CML7 will allow us to obtain deeper insights into the cellular events that this protein participates in and to determine its selectivity and mechanism of action.

Acknowledgments

We thank Prof. A Costa (University of Milan) for his precious help with confocal analysis, which was carried out at the NOLIMITS imaging facility at the University of Milan. We also thank the Centro Piattaforme Tecnologiche of the University of Verona for providing access to the NMR spectrometer, nanoITC calorimeter, and CD spectropolarimeter. This work has been partially supported by the italian MIUR-PRIN 2017 grant No. 2017ZBBYNC (to AA, MCB, ADM).

Appendix A. Supplementary data

Supplementary data to this article can be found online at https://doi.org/10.1016/j.jinorgbio.2019.110796.

References

[1] E.A. Permyakov, R.H. Kretsinger, Calcium Binding Proteins, John Wiley & Sons, Inc., 2010, pp. 567–573.
[2] E. McCormack, J. Braam, New Phytologist 159 (2003) 585–598, https://doi.org/10.1046/j.1469-8137.2003.00845.x.
[3] B. Boonburapong, T. Buaboocha, BMC Plant Biology 7 (2007) 4 BioMed Central, London.
[4] S. Munir, M.R.G. Khan, J. Song, S. Munir, Y. Zhang, Z. Ye, T. Wang, Plant Physiol. Biochem. 102 (2016) 167–179.
[5] K. Zhang, D. Yue, W. Wei, Y. Hu, J. Feng, Z. Zou, Frontiers in Plant Science, vol. 7, Frontiers Media S.A. (2016) 1820.
[6] E. Vandelle, A. Vannozzi, D. Wong, D. Danzi, A.M. Digby, S. Dal Santo, A. Astegno, Plant Physiol. Biochem. 129 (2018) 221–237.
[7] N. Guo, G. Wang, M. Zong, S. Han, F. Liu, Gene 677 (2018) 232–244.
[8] R. Vallone, V. La Verde, M. D'Onofrio, A. Giorgetti, P. Dominici, A. Astegno, Protein Sci. 25 (2016) 1461–1471.
[9] K.W. Bender, S. Dobney, A. Ogunrinde, D. Chiasson, R.T. Mullen, H.J. Teresinski, P. Singh, K. Munro, S.P. Smith, W.A. Snedden, Biochem. J. 457 (2014) 127–136.
[10] S. Dobney, D. Chiasson, P. Lam, S.P. Smith, W.A. Snedden, J. Biol. Chem. 284 (2009) 31647–31657.
[11] S.S. Scholz, J. Vadassery, M. Heyer, M. Reichelt, K.W. Bender, W.A. Snedden, W. Boland, A. Mithofer, Mol. Plant 7 (2014) 1712–1726.
[12] V. La Verde, P. Dominici, A. Astegno, Int. J. Mol. Sci. 19 (2018) 1331.
[13] A. Ogunrinde, K. Munro, A. Davidson, M. Ubaid, W.A. Snedden, Front. Plant Sci. 8 (2017) 2175.
[14] V. La Verde, M. Trande, M. D'Onofrio, P. Dominici, A. Astegno, Int. J. Biol. Macromol. 108 (2018) 1289–1299.
[15] A. Astegno, M.C. Bonza, R. Vallone, V. La Verde, M. D'Onofrio, L. Luoni, B. Molesini, P. Dominici, J. Biol. Chem. 292 (2017) 15049–15061.
[16] K.M. Cho, H.T. Nguyen, S.Y. Kim, J.S. Shin, D.H. Cho, S.B. Hong, S.H. Ok, New Phytol. 209 (2) (2016) 664–678.
[17] T. Yamaguchi, G.S. Aharon, J.B. Sottosanto, E. Blumwald, Proc. Natl. Acad. Sci. U. S. A. 102 (2005) 16107–16112.
[18] S.C. Popescu, G.V. Popescu, S. Bachan, Z. Zhang, M. Seay, M. Gerstein, M. Snyder, S.P. Dinesh-Kumar, Proc. Natl. Acad. Sci. U. S. A. 104 (2007) 4730–4735.
[19] A. Perochon, S. Dieterle, C. Pouzet, D. Aldon, J.P. Galaud, B. Ranty, Biochem. Biophys. Res. Commun. 398 (2010) 747–751.
[20] D. Aldon, M. Mbengue, C. Mazars, J.-P. Galaud, Int. J. Mol. Sci. 19 (2018) 665.
[21] A. Perochon, D. Aldon, J.P. Galaud, B. Ranty, Biochimie 93 (2011) 2048–2053.
[22] B. Ranty, D. Aldon, V. Cotelle, J.-P. Galaud, P. Thuleau, C. Mazars, Frontiers in plant science, vol. 7, Frontiers Media S.A. (2016) 327.
[23] S. Nie, M. Zhang, L. Zhang, BMC Genomics 18 (2017) 842.
[24] X. Zhu, C. Dunand, W. Snedden, J.-P. Galaud, Trends Plant Sci. 20 (2015) 483–489.
[25] E. de Castro, C.J. Sigrist, A. Gattiker, V. Bulliard, P.S. Langendijk-Genevaux, E. Gasteiger, A. Bairoch, N. Hulo, Nucleic Acids Res. 34 (2006) W362–W365.
[26] J.L. Gifford, M.P. Walsh, H.J. Vogel, Biochem. J. 405 (2007) 199–221.
[27] S.K. Won, Y.J. Lee, H.Y. Lee, Y.K. Heo, M. Cho, H.T. Cho, Plant Physiol. 150 (3) (2009) 1459–1473, https://doi.org/10.1104/pp.109.140905.
[28] B.M. Waters, New Phytol. 190 (2011) 510–513.
[29] M.C. Bonza, G. Loro, S. Behera, A. Wong, J. Kudla, A. Costa, Plant Physiol. 163 (3) (2013) 1230–1241, https://doi.org/10.1104/pp.113.226050.
[30] M.M. Bradford, Anal. Biochem. 72 (1976) 248–254.
[31] H. Gut, P. Dominici, S. Pilati, A. Astegno, M.V. Petoukhov, D.I. Svergun, M.G. Grütter, G. Capitani, J. Mol. Biol. 392 (2009) 334–351.
[32] V. Marino, A. Astegno, M. Pedroni, F. Piccinelli, D. Dell'Orco, Nanoscale 6 (2014) 412–423.
[33] A. Astegno, V. La Verde, V. Marino, D. Dell'Orco, P. Dominici, Biochimica et Biophysica Acta (BBA) - Proteins and Proteomics 1864 (2016) 297–307.
[34] A. Allegrini, A. Astegno, V. La Verde, P. Dominici, J. Biochem. 161 (2017) 349–360.
[35] A. Astegno, A. Giorgetti, A. Allegrini, B. Cellini, P. Dominici, Biomed. Res. Int. 2013 (2013) 701536.
[36] A. Astegno, E. Maresi, M. Bertoldi, V. La Verde, A. Paiardini, P. Dominici, Biochem. J. 474 (2017) 939–955.
[37] S.-D. Yoo, Y.-H. Cho, J. Sheen, Nat. Protoc. 2 (7) (2007) 1565–1572 PubMed PMID: 17585298.
[38] E. Teardo, L. Carraretto, S. Wagner, E. Formentin, S. Behera, S. De Bortoli, V. Larosa, P. Fuchs, F. Lo Schiavo, A. Raffaello, R. Rizzuto, A. Costa, M. Schwarzländer, I. Szabò, Plant Physiol. 173 (2017) 1355–1370.
[39] K. Arnold, L. Bordoli, J. Kopp, T. Schwede, Bioinformatics 22 (2006) 195–201.
[40] P. Benkert, M. Biasini, T. Schwede, Bioinformatics 27 (2011) 343–350.
[41] S.T. Rao, S. Wu, K.A. Satyshur, M. Sundaralingam, K.-Y. Ling, C. Kung, Protein Sci. 2 (1993) 436–447.
[42] C. Combet, C. Blanchet, C. Geourjon, G. Deléage, Trends Biochem. Sci. 25 (2000) 147–150.
[43] J.L. Gifford, M. Jamshidiha, J. Mo, H. Ishida, H.J. Vogel, Plant Cell 25 (2013) 4512–4524.
[44] S. Ohki, M. Ikura, M. Zhang, Biochemistry 36 (1997) 4309–4316.
[45] M. Ikura, O. Minowa, K. Hikichi, Biochemistry 24 (1985) 4264–4269.
[46] A. Malmendal, G. Carlstrom, C. Hambraeus, T. Drakenberg, S. Forsen, M. Akke, Biochemistry 37 (8) (1998) 2586–2595.
[47] M. Zhang, T. Tanaka, M. Ikura, Nat. Struct. Biol. 2 (1995) 758–767.
[48] S.M. Gagne, S. Tsuda, M.X. Li, M. Chandra, L.B. Smillie, B.D. Sykes, Protein Sci. 3 (1994) 1961–1974.
[49] R. Gilli, D. Lafitte, C. Lopez, M. Kilhoffer, A. Makarov, C. Briand, J. Haiech, Biochemistry 37 (1998) 5450–5456.
[50] R. Dagher, S. Peng, S. Gioria, M. Fève, M. Zeniou, M. Zimmermann, C. Pigault, J. Haiech, M.-C. Kilhoffer, Biochimica et Biophysica Acta (BBA) - Molecular Cell Research 1813 (2011) 1059–1067.
[51] S. Mukherjee, P.M. Mohan, K.V. Chary, Biochemistry 46 (2007) 3835–3845.
[52] G. Wu, Z. Gao, A. Dong, S. Yu, Int. J. Biol. Macromol. 50 (2012) 1011–1017.
[53] S. Linse, P. Brodin, C. Johansson, E. Thulin, T. Grundstrom, S. Forsen, Nature 335 (1988) 651–652.
[54] S. Linse, A. Helmersson, S. Forsen, J. Biol. Chem. 266 (1991) 8050–8054.
[55] M. Comte, Y. Maulet, J.A. Cox, The Biochemical journal 209 (1983) 269–272.
[56] S.H. Seeholzer, M. Cohn, J.A. Putkey, A.R. Means, H.L. Crespi, Proc. Natl. Acad. Sci. 83 (1986) 3634–3638.
[57] B. Kuhlman, H.Y. Yang, J.A. Boice, R. Fairman, D.P. Raleigh, J. Mol. Biol. 270 (1997) 640–647.
[58] J.S. Smith, J.M. Scholtz, Biochemistry 37 (1998) 33–40.
[59] A. Astegno, E. Maresi, V. Marino, P. Dominici, M. Pedroni, F. Piccinelli, D. Dell'Orco, Nanoscale 6 (2014) 15037–15047.
[60] M. Ikura, G.M. Clore, A.M. Gronenborn, G. Zhu, C.B. Klee, A. Bax, Science 256 (1992) 632–638.
[61] W.E. Meador, A.R. Means, F.A. Quiocho, Science 257 (1992) 1251–1255.
[62] C.H. Yun, J. Bai, D.Y. Sun, D.F. Cui, W.R. Chang, D.C. Liang, Acta Crystallogr D Biol Crystallogr 60 (2004) 1214–1219.
[63] S. Kumar, M. Mazumder, N. Gupta, S. Chattopadhyay, S. Gourinath, FEBS Lett. 590 (2016) 3029–3039.
[64] M. Ikura, J.B. Ames, Proc. Natl. Acad. Sci. U. S. A. 103 (2006) 1159–1164.
[65] A. Villarroel, M. Taglialatela, G. Bernardo-Seisdedos, A. Alaimo, J. Agirre, A. Alberdi, C. Gomis-Perez, M.V. Soldovieri, P. Ambrosino, C. Malo, P. Areso, J. Mol. Biol. 426 (15) (2014) 2717–2735.
[66] M.A. Wilson, A.T. Brunger, J. Mol. Biol. 301 (2000) 1237–1256.
[67] X. Zhu, C. Dunand, W. Snedden, J.P. Galaud, Trends Plant Sci. 20 (2015) 483–489.
[68] H. Tidow, P. Nissen, FEBS J. 280 (2013) 5551–5565.
[69] F. Spyrakis, A. BidonChanal, X. Barril, F.J. Luque, Curr. Top. Med. Chem. 11 (2011) 192–210.
[70] K.W. Bender, W.A. Snedden, Plant Physiol. 163 (2013) 486–495.
[71] H. Zeng, L. Xu, A. Singh, H. Wang, L. Du, B.W. Poovaiah, Frontiers in Plant Science, vol. 6, Frontiers Media S.A, 2015, p. 600.
[72] T.A. DeFalco, K.W. Bender, W.A. Snedden, Biochem. J. 425 (2010) 27–40.
[73] C. Cheval, D. Aldon, J.-P. Galaud, B. Ranty, Biochimica et Biophysica Acta (BBA) - Molecular Cell Research 1833 (2013) 1766–1771.
[74] S. Linse, S. Forsen, Adv. Second Messenger Phosphoprotein Res. 30 (1995) 89–151.
[75] A. Malmendal, J. Evenas, S. Forsen, M. Akke, J. Mol. Biol. 293 (1999) 883–899.
[76] A. Malmendal, J. Evenas, E. Thulin, G.P. Gippert, T. Drakenberg, S. Forsen, J. Biol. Chem. 273 (1998) 28994–29001.
[77] Z. Grabarek, Biochim. Biophys. Acta 1813 (2011) 913–921.
[78] K.T. O'Neil, W.F. DeGrado, Trends Biochem. Sci. 15 (1990) 59–64.
[79] A. Scaloni, N. Miraglia, S. Orrù, P. Amodeo, A. Motta, G. Marino, P. Pucci, J. Mol. Biol. 277 (1998) 945–958.
[80] A.M. Weljie, H.J. Vogel, Protein Eng. 13 (2000) 59–66.